minerals

MDPI

Article

Geochronological Study of the Jiashengpan Zn–Pb Deposit in Northern China: Implications for Base Metal Mineralization in Collisional Orogens

Chang Yu [1], Ri-Chen Zhong [1,*], Yu-Ling Xie [1] and Wen-Bo Li [2]

[1] School of Civil and Resource Engineering, University of Science and Technology Beijing, Beijing 100083, China; yuchangustb@126.com (C.Y.); yulingxie63@hotmail.com (Y.-L.X.)

[2] Key Laboratory of Orogenic Belt and Crustal Evolution, Peking University, Beijing 100871, China; liwenbo@pku.edu.cn

* Correspondence: zhongrichen@126.com

Received: 20 August 2019; Accepted: 7 October 2019; Published: 9 October 2019

Abstract: The Jiashengpan Zn–Pb deposit is located in the Langshan-Zhaertai region of the North China Craton. Zinc-lead mineralization at the Jiashengpan shows characteristics of shear-zone controlled syn-metamorphic mineralization. The $^{39}Ar/^{40}Ar$ ages of syn-ore hydrothermal muscovite averages at ~380 Ma, suggesting that the Zn–Pb mineralization took place in the Devonian. These results agree with zircon U–Pb ages of post-ore granite, which constrain the ore formation to be older than 277 ± 2 Ma. Ore formation was coeval with the emplacement of regional orogenic belts that formed as result of subduction associated with the closure of the eastern Paleo-Asian Ocean (~400 Ma). The Jiashengpan deposit provides evidence for base metal mineralization associated with metamorphogenic and shear-zone controlled characteristics during continental-continental collision, stressing the significance of orogenic activities for enrichment of base metals.

Keywords: Jiashengpan; Langshan-Zhaertai; Zircon U–Pb; Muscovite $^{39}Ar/^{40}Ar$; ore enrichment; ore remobilization; metamorphic fluids

1. Introduction

The Langshan-Zhaertai region in western Inner Mongolia is located along the northern margin of the North China Craton (NCC). This area is a significant Cu–Zn–Pb polymetallic ore belt hosting several Zn–Pb–(Cu) deposits, including the giant Dongshengmiao deposit and the Huogeqi, Tanyaokou, and the Jiashengpan deposits. The Jiashengpan Zn–Pb polymetallic deposit developed in rift sedimentary rocks in the Mesoproterozoic Era, and has traditionally been regarded as a syngenetic strata-bound or sedimentary exhalative deposit [1–4]. However, some researchers have noted that deformation, such as thrust faulting, of ore-hosting rift sequences had significant control of the formation of Zn–Pb orebodies [5].

More recently, our studies on field geology, petrography, and mineral geochemistry [6] revealed that the Jiashengpan deposit has undergone a two-stage genesis in which (i) syngenetic processes (during sedimentation or diagenesis of the host rocks) lead to pre-enrichment of Zn and Pb, forming Zn–Pb-bearing but sub-economic rift sedimentary rocks, and (ii) syngenetic sulfides were subsequently remobilized by metamorphic fluids, migrated, and concentrated along shear zones, resulting in high-grade Zn–Pb mineralization.

This ore-forming history may represent an important mechanism of epigenetic base metal mineralization, i.e., ore-formation via syn-metamorphic enrichment of pre-enriched but sub-economic metals. This may partly account for the presence of the so-called orogenic-type base metal deposits [7–9],

the formation of which is difficult to explain by current orogenic Au deposit formation theories (i.e., the "gold-only" paradox; [10,11]).

It is readily accepted that metamorphism and deformation processes played a decisive role in the formation of the Jiashengpan deposit by controlling the spatial distribution and geological characteristics of the orebodies. However, the age and geodynamic background of the remobilization/mineralization process remains unclear. In this study, the ore formation age of the Jiashengpan deposit was determined by $^{39}Ar/^{40}Ar$ dating of syn-ore muscovite and U–Pb dating of zircon from post-ore granite. Geochronological data reveal that the Jiashengpan deposit was formed in a continent-continent collisional setting, is considered atypical for Zn–Pb mineralization, and thus, may represent an alternative source for base metal resources. The mechanism controlling the formation of this type of mineralization is a focus of this paper.

2. Regional Geology

The Langshan-Zhaertai polymetallic ore belt extends approximately 600 km from west to east along the western segment of the northern margin of the NCC. The Archean crystalline basement of the NCC exposed in this area is composed of high-grade (amphibolite-granulite facies) metamorphic rocks, locally known as the Wulashan Group in the west (the Langshan area) and the Wutai Group in the east (the Zhaertai area) (Figure 1).

During the Proterozoic, rift sediments with intercalated volcanic rocks were emplaced throughout the entire area, unconformably overlying the Archean basement, and later underwent sub-greenschist to lower amphibolite facies metamorphism [2] (Figure 1). Both the Langshan and the Zhaertai Groups were regarded as Mesoproterozoic strata deposited in an integral rift in previous studies [12]. However, more recent work indicates that the Langshan Group was deposited during the Neoproterozoic [13], whereas the Zhaertai Group is Mesoproterozoic in age [14,15], suggesting that these groups might have different tectonic affinities during the Proterozoic. In the west, the depositional age of the Langshan Group is constrained to be younger than ~1100 Ma by U–Pb dating of detrital zircons separated from metasedimentary rocks [14], and zircon U–Pb dating from intercalated metavolcanic rocks that yield an age of eruption of 810 Ma [13,16]. In the east, the emplacement of the Zhaertai Group is constrained to be Mesoproterozoic in age, based on the ages of detrital zircon from metasedimentary rocks that range from 2.5 to 1.8 Ga [14], and the U–Pb dating result of a single zircon grain separated from a basaltic metavolcanic rock of 1743 ± 7 Ma [15].

This area remained tectonically active from the late Paleozoic until the early Mesozoic. Carbonaceous to Triassic plutonic intrusions were widely developed through the Langshan-Zhaertai areas, with lithologies ranging from diorite to granite [17–22] (Figure 1). A series of east to west-trending thrust faults and shear zones were also developed in response to the tectonic activity (Figure 1).

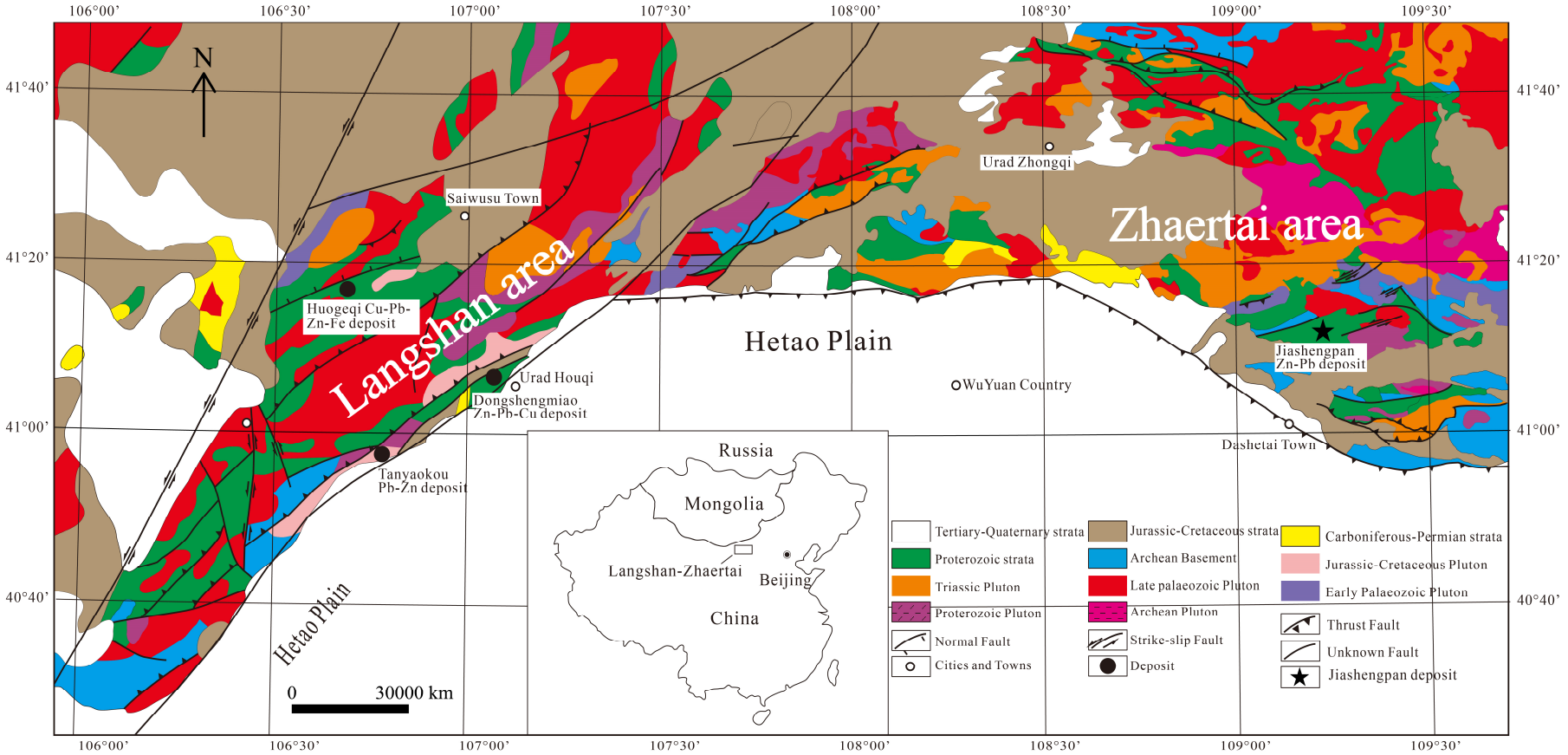

Figure 1. Regional geology of Langshan-Zhaertai district (modified from 1:500,000 regional geological map provided by the Bureau Geological Mineral Exploration and Development in Inner Mongolia).

The geodynamic background of the late Paleozoic to early Mesozoic magmatism and tectonism are under debate. One school of thought, based mainly on the "arc-like" geochemical characteristics of Carboniferous-Permian intrusions, proposes that this activity resulted from the prolonged subduction of the Paleo-Asian Ocean (PAO) beneath the NCC, with the final enclosure of the ocean basin taking place at the end of the Permian to early Triassic [23–25]. In recent years, growing evidence from sedimentology, paleomagnetism, and paleontology show that the PAO was closed as early as the Devonian [26], and the late Paleozoic magmatic and tectonic events took place in a post-collisional extensional environment [21,27]. Marine sediments with Late Paleozoic ages are regarded to have formed in the shallow water environment of a small basin, rather than the PAO [28,29]. This small basin is believed to have formed as a response to post-collisional extension, and was subsequently closed during the end of the Permian to early Triassic [27,30–34]. Furthermore, several Late Paleozoic intrusions, initially thought to have formed in subduction environments, have been re-interpreted as products of post-collisional extension by more recent petrological studies [20,33].

Following the closure of the PAO, the collision between the NCC and the South Mongolian microcontinent (SMM) lead to regional compression and crustal thickening, and thus, the development of a Barrovian metamorphic belt in this area [35]. The age of metamorphism recorded by metamorphic zircon grains ranges between 412 to 374 Ma, with a weighted average of 399 ± 6 Ma [31].

3. Geology of Jiashengpan Deposit

The Jiashengpan deposit is located in the eastern region (the Zhaertai area) of the Langshan-Zhaertai metallogeny belt, with metal reserves of 1.68 Mt Zn at an average grade of 3.95%, and 0.19 Mt Pb at 1.35%. In addition to Zn–Pb orebodies, massive pyrite is mined as an S resource. Lead-zinc orebodies at the Jiashengpan consistently dip north with strikes of ~350° and dip angles of ~70°, similar to the occurrence of the F1 fault (Figures 2 and 3). The main strata exposed in the mining area include the Archean Wutai Group, the Mesoproterozoic Zhaertai Group, and rare Permian and Cretaceous sediments (Figure 2). The Archean Wutai Group is part of the crystalline basement of the NCC, consisting of gneiss and migmatite.

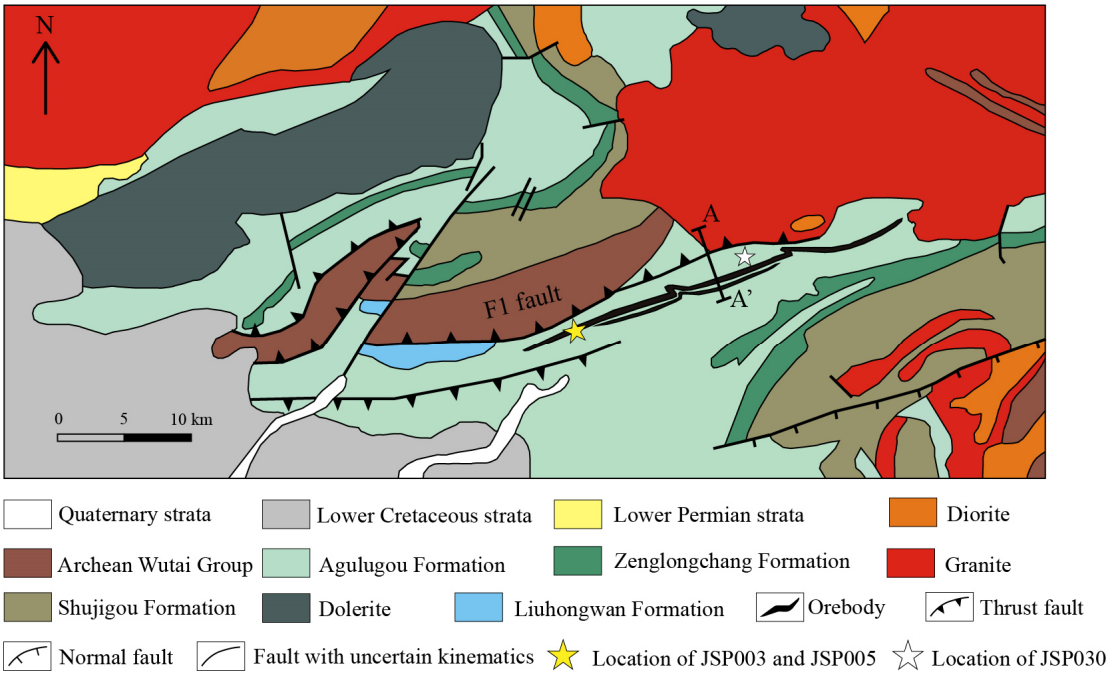

Figure 2. Geological map of the Jiashengpan deposit; modified from [4].

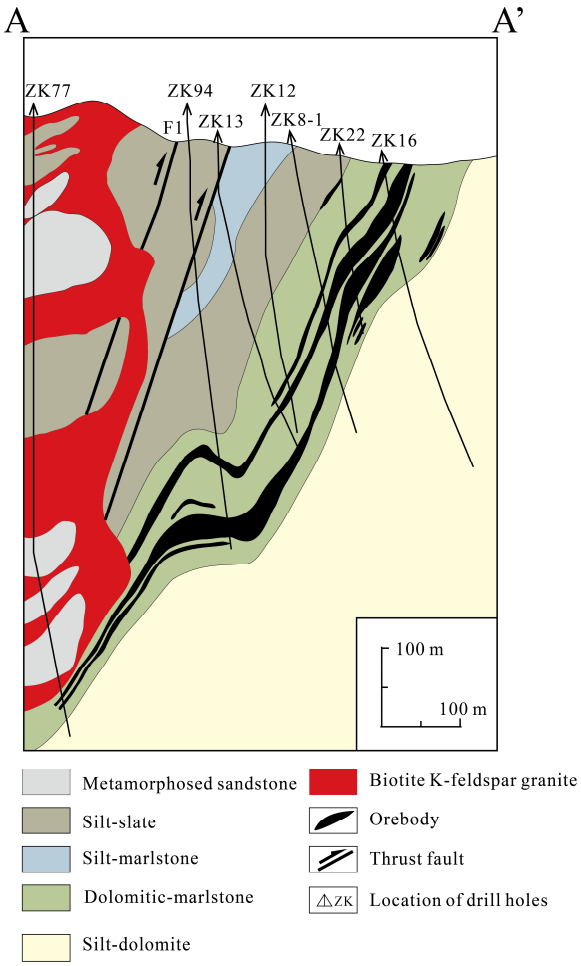

Figure 3. Cross section of A-A' in Figure 2 (modified from the map provided by Jiashengpan Mining Ltd.).

The orebodies at the Jiashengpan are all hosted in the Agulugou Formation of Zhaertai Group, with immediate host rocks consisting mainly of carbonaceous shale, marlstone, and dolomite, with some units having high contents of organic matter [1,4]. The Agulugou Formation can be further divided into three lithological units from bottom to top. The first and third units are rich in K_2O, SiO_2, and Al_2O_3 contents, and the second units are rich in MgO, SiO_2, MnO, and FeO abundances. These lithologies underwent sub-greenschist to lower greenschist facies metamorphism.

Thrust faults are widely developed within the Jiashengpan deposit. Among them, the F1 thrust fault, separating the Wutai Group in the northern and the Zhaertai Group in the south, is the best developed and most representative (Figure 2), with an average trend of 334° and dip angle of 61°. A shear zone developed concurrently with the fault, and mylonites were broadly formed nearby.

The main intrusions exposed in the Jiashengpan deposit consist of late Paleozoic biotite K-feldspar granite. This granite truncates the F1 fault and ore bodies underground. In addition, several diorite, granite, and granite-porphyry stocks are exposed in the mining area (Figure 3; [4]).

A previous study [6] proposed a two-stage model for the formation of the Jiashengpan deposit, and it is summarized below. The early-stage sulfides are characterized by the widely developed massive pyrite with fine-grained textures or framboidal structure, indicating a sedimentary origin. Moreover, syngenetic Zn–Pb-sulfides were observed as disseminated fine grains in dolomite, and in general, were of no economic interest. All the economically important Zn–Pb ores were formed during the late-stage mineralization, with pyrite and pyrrhotite and hydrothermal gangue minerals such as quartz, calcite, and dolomite. The late-stage mineralization shows characteristics of shear

zone-controlled mineralization, such as mineral precipitation following mylonitic foliations of the host rocks.

4. Materials and Methods

4.1. Muscovite $^{39}Ar/^{40}Ar$ Dating

In this study, samples JSP003 and JSP005 for muscovite $^{39}Ar/^{40}Ar$ analysis were separated from Zn–Pb ores collected from the western ore block of the Jiashengpan deposit, and their locations are identified in Figure 2. Sample JSP003 is a vein-type ore (Figure 4A), composed mainly of coarse-grained quartz, muscovite, biotite, and sulfides (Figure 4B,C). Hydrothermal minerals from sample JSP005 (Figure 4D) are mainly sphalerite, muscovite, and quartz, with minor biotite, pyrite, pyrrhotite, and galena (Figure 4E,F). These minerals form the matrix that cements tectonically brecciated massive pyrite (Figure 4D).

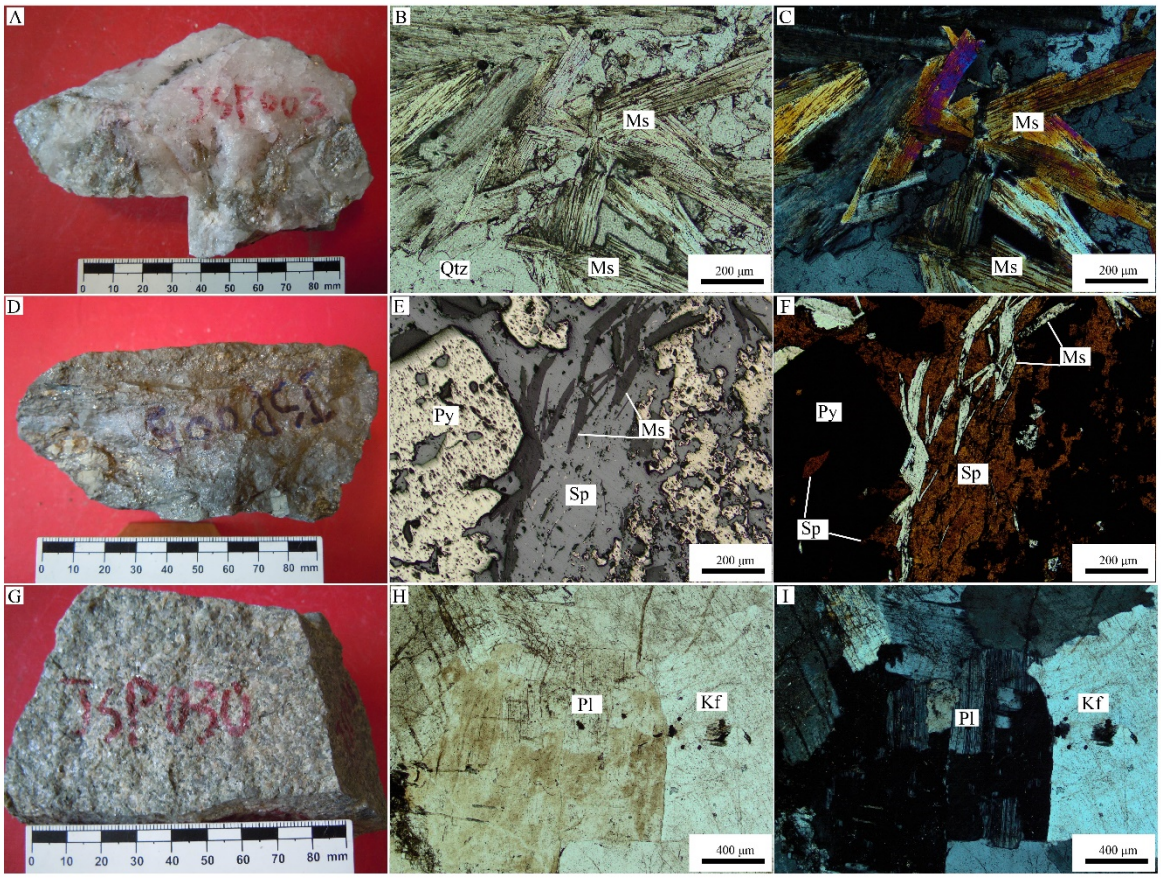

Figure 4. Petrographic characteristics of analyzed ore samples JSP003, JSP005, and JSP030 from the post-mineralization biotite K-feldspar granite at the Jiashengpan deposit. (**A**) Syn-ore quartz vein, hand specimen (sample JSP003); (**B**) hydrothermal quartz coexisting with muscovite, plane-polarized light (JSP003); (**C**) the same field of view as shown in (**B**), cross-polarized light; (**D**) zinc-lead ore, hand specimen (sample JSP005); (**E**) syn-ore hydrothermal muscovite coexisting with hydrothermal sphalerite, reflected light (JSP005); (**F**) the same field of view as shown in (**E**), plane-polarized light (JSP005); (**G**) biotite K-feldspar granite, hand specimen (sample JSP030); (**H**) feldspar and plagioclase are coexistent, plane-polarized light (JSP030); (**I**) the same field of view as shown in (**H**), cross-polarized light (JSP030). Abbreviations: Qtz = quartz, Py = pyrite, Ms = muscovite, Sp = sphalerite, Kf = feldspar, and Pl = plagioclase.

$^{39}Ar/^{40}Ar$ geochronologic analysis of muscovite was performed at the State Key Laboratory of Lithospheric Evolution, Institute of Geology and Geophysics, Chinese Academy of Sciences. Muscovite separated from ores was first covered with aluminum foil and enclosed in cadmium-coated vacuum quartz vials with Bern4M standards (18.69 ± 0.07 Ma; [36]). Samples were then irradiated for 24 h at the H8 position of the reactor at the Beijing Atomic Energy Research Institute (49–2) and heated at 600 °C for 30 min in a Ta crucible. Step-heating experiments were carried out at temperatures of 700 °C or 750 °C to 1400 °C or 1500 °C with an interval of 40–50 °C at the Institute of Geology and Geophysics, Chinese Academy of Sciences in Beijing. Gases produced during the heating process were analyzed by an MM5400 mass spectrometer. Crystals of K_2SO_4 and CaF_2 were used to obtain correction factors for K and Ca, with $[^{36}Ar/^{37}Ar]_{Ca}$ = 0.000271, and $[^{39}Ar/^{37}Ar]_{Ca}$ = 0.000652. Plateau ages were calculated using ArArCALC [37] and were defined using the criteria of Dalrymple and Lanphere [38] and Fleck et al. [39].

4.2. Zircon U–Pb Dating

The sample JSP030 for zircon U–Pb dating was collected from biotite K-feldspar granite that intruded into the orebody in the underground working site of the mine (Figure 4G), and the sample location is shown in Figure 2. The sample has a granitic texture, and is composed mainly of K-feldspar, plagioclase, quartz, and biotite (Figure 4H,I). Plagioclase and K-feldspar are subhedral with grains sizes of 0.5–5 mm. Quartz is anhedral, with sizes ranging from 0.3–2 mm, and biotite is predominantly fine-grained (0.2–1 mm).

Zircon was separated using conventional density and magnetic separation techniques, and then handpicked under a binocular microscope. Zircon crystals were mounted in epoxy for polishing. Their internal structure was examined using an optical microscope and cathodoluminescence (CL) imaging techniques prior to U–Pb dating. Zircon U–Pb dating was performed using an Elan 6100 DRC quadrupole mass spectrometer coupled with a Geolas200M Laser-Ablation System at the State Key Laboratory of Geological Processes and Mineral Resources, China University of Geosciences, Wuhan, China. Detailed analytical conditions and the method of data reduction are similar to those described by Yuan et al. [40]. Zircon U–Th–Pb measurements were made on 32 μm diameter spots on single grains. NIST 610 was used as an internal standard for the analyses and zircon GJ-1 was used as the external calibration standard. Common lead was corrected using the method of Andersen [41], isotopic ratios and element concentrations were calculated using ICP-MS DataCal software [42], and crystallization ages were calculated using ISOPLOT 4.0 [43].

5. Results

Step-wise heating results for muscovites selected for $^{39}Ar/^{40}Ar$ analysis are shown in Table 1. Muscovites separated from sample JSP003 yielded a fairly flat age spectrum with a well-defined plateau at an age of 387.7 ± 2 Ma (MSWD = 0.31), corresponding to four stages and 85.7% ^{39}Ar release (Figure 5A). Sample JSP005 produced a muscovite $^{39}Ar/^{40}Ar$ age of 373.2 ± 1.9 Ma (MSWD = 0.18), with a plateau of three stages and 66.1% ^{39}Ar release (Figure 5C). Two isochron ages of 388.0 ± 2.9 Ma and 372.9 ± 2.6 Ma were also obtained from the two samples, with initial $^{40}Ar/^{36}Ar$ ratios of 283 ± 53 and 306 ± 66 for sample JSP003 and 005, respectively (Figure 5B,D).

Petrological observations indicate that muscovite grains in these samples are coeval with hydrothermal sphalerite, sulfides, and quartz characteristics of formation during a syn-ore stage (Figure 4B,D). Gangue minerals accompanying muscovite and Zn–Pb sulfides are mainly quartz, dolomite, and chlorite, with a minor amount of biotite (Figure 4F; [6]), an assemblage that is stable at temperatures close to the closure temperature for muscovite (~350 °C). The flat age spectra of the two samples shown in Figure 5A,C suggest that they did not undergo post-ore formation disturbance [44], which is in agreement with the observation that the syn-ore minerals are generally free from deformation and recrystallization, excluding the possibilities of post-ore thermal disturbance and age reset. Therefore, the mid to late Devonian muscovite $^{39}Ar/^{40}Ar$ ages are considered representative of the time of sulfide precipitation.

Table 1. $^{40}Ar/^{39}Ar$ step-heating data of sample JSP003 and JSP005 at the Jiashengpan deposit.

Step	$^{40}Ar/^{39}Ar$	$^{37}Ar/^{39}Ar$	$^{36}Ar/^{39}Ar$	$^{40}Ar^*/^{39}Ar$	$^{40}Ar^*$ (%)	Age (Ma)	± 2σ
JSP003 J = 0.005245							
Step 1	23.9677	2.760084	0.02740485	16.11258	67.10	146.36	± 51.27
Step 2	34.12551	1.679184	0.02029718	28.28611	82.79	249.56	± 13.20
Step 3	42.36354	0.8150739	0.01561427	37.82787	89.24	326.52	± 3.53
Step 4	48.12279	0.2661296	0.00833339	45.68248	94.91	387.50	± 0.96
Step 5	46.60529	0.1278701	0.00300451	45.72448	98.10	387.82	± 0.50
Step 6	47.49956	0.117464	0.00623654	45.66253	96.12	387.34	± 1.01
Step 7	47.14671	0.1748673	0.0048883	45.71441	96.95	387.74	± 0.41
Step 8	46.65878	0.2208983	0.00059775	46.4995	99.64	393.72	± 0.45
Step 9	46.09346	0.5585837	0.00846844	43.64464	94.65	371.87	± 2.61
Step 10	43.59298	1.199543	0.00398998	42.53624	97.49	363.32	± 2.83
Step 11	39.86405	1.560482	0.0123677	36.36434	91.12	314.93	± 6.55
JSP005 J = 0.005264							
Step 1	25.4155	3.873548	3.873548	19.25437	75.567	174.1679	± 10.78296
Step 2	36.61591	0.9012945	0.9012945	33.29723	90.8831	291.3648	± 1.793558
Step 3	42.81073	0.4183343	0.4183343	41.35762	96.5794	355.3477	± 0.7686522
Step 4	43.94439	0.1664867	0.1664867	43.63443	99.2839	373.0172	± 0.8833513
Step 5	44.85159	0.109381	0.109381	43.69164	97.4069	373.459	± 1.23016
Step 6	45.16053	0.1512399	0.1512399	43.66126	96.6706	373.2244	± 0.6035693
Step 7	44.95598	0.382604	0.382604	44.41771	98.778	379.0562	± 1.71614
Step 8	44.8162	0.7196377	0.7196377	43.03958	95.9907	368.4174	± 3.699181
Step 9	42.65749	0.7507671	0.7507671	42.42905	99.4158	363.6842	± 3.81958
Step 10	38.1425	1.67781	1.67781	37.31152	97.7144	323.5136	± 3.241947

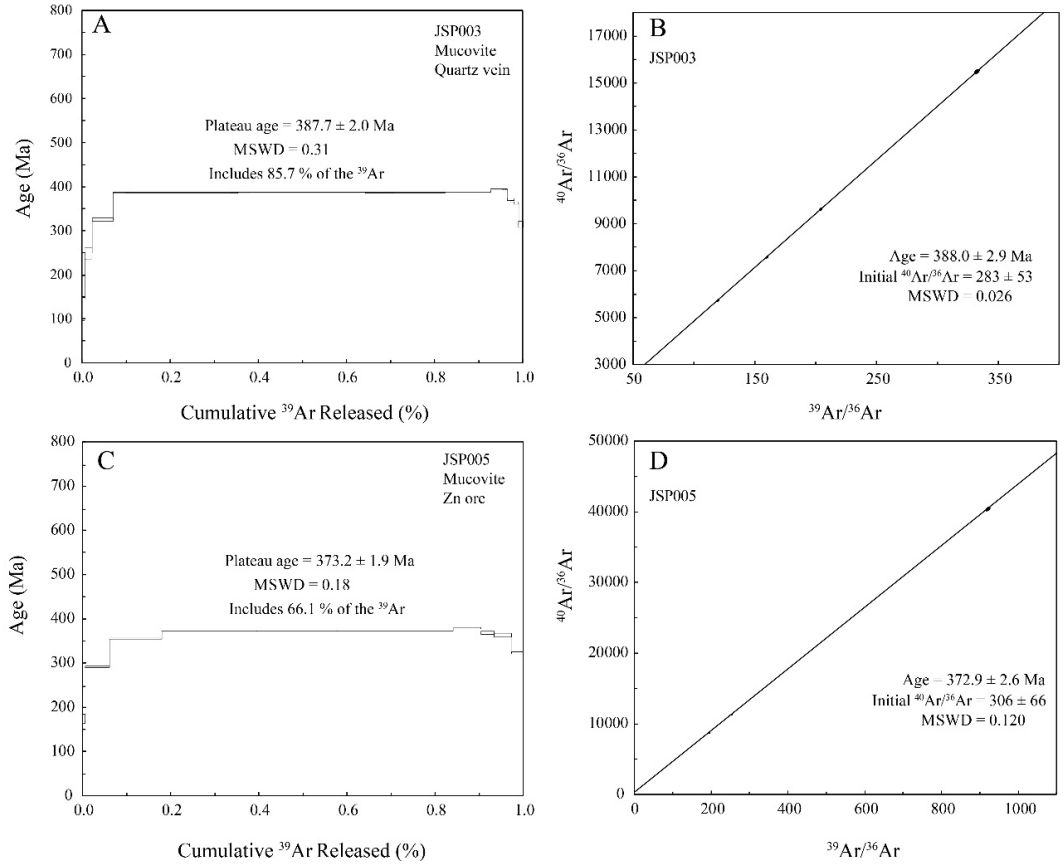

Figure 5. $^{40}Ar/^{39}Ar$ plateau and isochron ages of muscovite samples (JSP003 and 005) from the Jiashengpan deposit. (**A**) Plateau age of the muscovite separated from sample JSP003. (**B**) Isochron age of muscovite sample (JSP003). (**C**) Plateau age of the muscovite separated from sample JSP005. (**D**) Isochron age of muscovite sample (JSP005).

Results of U–Pb dating of zircon separated from sample JSP030 are listed in Table 2. The isotopic ratios of 12 analyzed grains form a tight cluster on the concordia diagram with the age of 278 ± 2.3 Ma (n = 12, MSWD = 0.92) and yield a weighted mean $^{206}Pb/^{238}U$ age of 277.2 ± 2.6 Ma (95% confidence level, MSWD = 1.8) (Figure 6). Zircons are characterized by euhedral or columnar morphologies, with well-developed oscillatory zoning observed under reflected light (Figure 7A). Under transmitted light, the grains appear clear (Figure 7B), yet under CL, they are not (Figure 7C). These features suggest a magmatic origin for the zircon grains, and no inherited zircons have been found. The magmatic genesis is also manifest by the Th/U ratios of the zircons, which range from 0.39 to 1.42 [45]. Therefore, the zircon U–Pb age is considered to be that of crystallization of the intrusion.

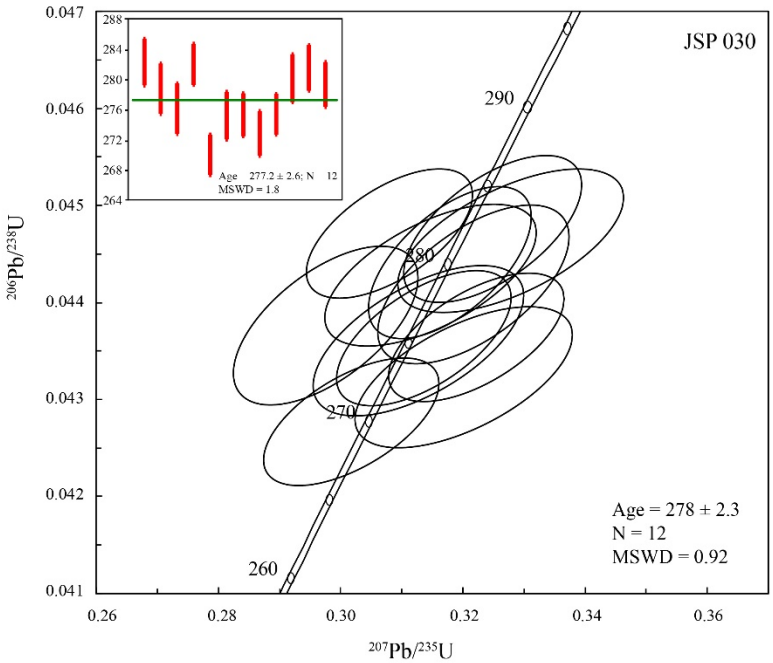

Figure 6. U–Pb Concordia diagram of zircon from the post-ore granite (JSP030).

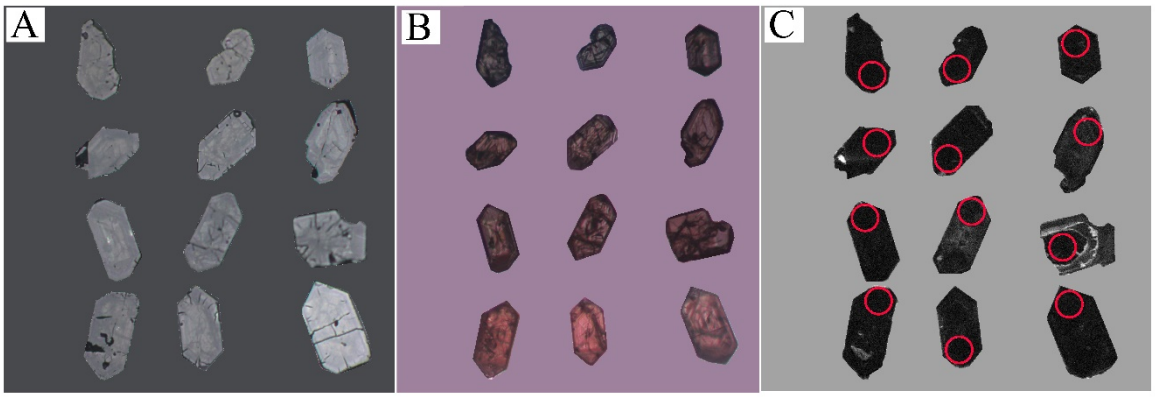

Figure 7. Petrographic characteristics of zircons from sample JSP030 and analyzed points. (**A**) Reflected light. (**B**) Transmitted light. (**C**) The cathodoluminescence image. Red circles indicate analysis points.

Table 2. LA-ICP-MS zircon U–Pb dating of biotite K-feldspar granite at the Jiashengpan deposit.

Spot	^{232}Th (ppm)	^{238}U (ppm)	^{207}Pb/^{206}Pb	^{207}Pb/^{206}Pb	^{207}Pb/^{235}U	^{207}Pb/^{235}U	^{206}Pb/^{238}U	^{206}Pb/^{238}U	^{207}Pb/^{206}Pb	^{207}Pb/^{206}Pb	^{207}Pb/^{235}U	^{207}Pb/^{235}U	^{206}Pb/^{238}U	^{206}Pb/^{238}U
			Ratio	1σ	Ratio	1σ	Ratio	1σ	Age (Ma)	1σ	Age (Ma)	1σ	Age (Ma)	1σ
JSP030-04	9275	12292	0.0518	0.0016	0.3249	0.0096	0.0448	0.0005	276	70	286	7	282	3
JSP030-05	3808	7592	0.0520	0.0017	0.3217	0.0103	0.0442	0.0005	283	78	283	8	279	3
JSP030-13	5842	9655	0.0487	0.0016	0.2975	0.0100	0.0438	0.0005	132	78	264	8	276	3
JSP030-15	9054	12744	0.0494	0.0014	0.3080	0.0090	0.0447	0.0004	165	69	273	7	282	3
JSP030-16	6800	9841	0.0506	0.0016	0.3017	0.0095	0.0428	0.0004	220	77	268	7	270	3
JSP030-19	2186	5396	0.0514	0.0019	0.3127	0.0114	0.0436	0.0005	261	85	276	9	275	3
JSP030-22	9025	11770	0.0513	0.0015	0.3136	0.0094	0.0436	0.0005	254	67	277	7	275	3
JSP030-24	2707	5643	0.0528	0.0020	0.3202	0.0117	0.0432	0.0005	317	118	282	9	273	3
JSP030-25	7089	10531	0.0564	0.0020	0.3429	0.0117	0.0432	0.0005	322	73	299	9	272	3
JSP030-27	7576	11011	0.0527	0.0016	0.3222	0.0095	0.0436	0.0004	250	68	284	7	275	3
JSP030-33	3033	4686	0.0509	0.0019	0.3147	0.0114	0.0443	0.0005	283	91	278	9	279	3
JSP030-37	5891	9535	0.0520	0.0021	0.3279	0.0122	0.0446	0.0005	235	87	288	9	282	3

6. Discussion

Based on the petrological observations, muscovite is coeval with ore minerals such as hydrothermal sphalerite, galena, pyrite, and quartz, with characteristics of formation coeval with Zn–Pb precipitation (Figure 4B,E). In addition, the temperature of Zn–Pb mineralization and muscovite precipitation was close to the closure temperature of muscovite. Therefore, the $^{39}Ar/^{40}Ar$ ages for muscovite can represent the age of Zn–Pb mineralization. The mineralization age at the Jiashengpan is close to the metamorphic age of the Baoyintu Group (~400 Ma; [31]), which is similar to dates for Proterozoic rift sequences in the western part of the Langshan-Zhaertai areas. The ~400 Ma metamorphism is interpreted as a result of continent-continent collision between NCC and SMM, following the final enclosure of the PAO [35]. This dating result indicates syn-metamorphic mineralization of the Jiashengpan deposit, consistent with fact that the assemblage of hydrothermal gangue minerals accompanying Zn–Pb mineralization is the same as the assemblage of metamorphic minerals in the host rocks [6]. Therefore, we conclude that the Zn–Pb mineralization resulted from metamorphic devolatilization of the ore-hosting rift sequences during the Devonian.

The Devonian ore-forming age is consistent with the constraint provided by the post-ore granite, which yields U–Pb zircon dates of ca. 278 Ma. Although magmatic rocks are common in the mining area, magmatism seems to have made no significant contribution to the mineralization at the Jiashengpan deposit. This is manifested by (i) the lack of identified magmatic activity coeval with the Devonian Zn–Pb mineralization at the mine site or adjacent areas, and (ii) the lack of overprinting mineralization, hydrothermal alteration, or mineral remobilization near the contacts between the intrusion and the orebodies.

The Jiashengpan deposit was formed in the Devonian and controlled by the orogenic activity, which was characterized by a compressional to transpressional stress field, crustal thickening, large regions of metamorphism, and lack of large-scale magmatism. However, it is not traditionally thought of as an ideal tectonic setting for Zn–Pb mineralization because the vast majority of the global Zn and Pb resources are related to circulation of sea water (e.g., SEDEX-type), injection of basinal brines (e.g., MVT-type), or hydrothermal activity following magmatism (e.g., skarn-type). On the contrary, this geologic setting is favorable for orogenic Au mineralization, which is widely perceived to be induced by movement of metamorphic fluids [10,46]. In the Zhaertai region, a large orogenic Au deposit (the Wulashan) has been confirmed to have a similar formation age (~350 Ma; [47–49]) to the Jiashengpan deposit. In contrast to Au, theoretically, base metals such as Zn, Pb and Cu have much weaker mobility during metamorphism [11,50], and thus base metal mineralization is much less common than that for Au during orogeny. The Jiashengpan Zn–Pb deposit, however, shares broad geological and geochemical similarities with the local orogenic Au deposit and formed in the tectonic setting of collision orogen.

Although the high-grade economic orebodies in this region formed as a result of Devonian metamorphism and tectonism, the majority of ore-forming metals at the Jiashengpan were firstly enriched during a syngenetic process coeval with the deposition of the ore-hosting Zhaertai Group [6]. This differs from the formation of orogenic Au, which necessitates the scavenging of gold from large volumes of source rocks with average crustal gold concentrations during regional metamorphism [10]. In the scenario of the Jiashengpan deposit, however, although the metamorphic fluid has only limited ability to transport base metals, it can largely facilitate short-range metal remobilization [51], leading to redistribution and enrichment of Zn and Pb. Thus, the Jiashengpan deposit is a case of a base metals ore body that formed via metal remobilization and enrichment during orogenic activity.

In addition to the Jiashengpan, many of the identified base metals deposits show characteristics of multi-stage mineralization or metal remobilization associated with orogenic activity, such as the Coeur d'Alene Ag–Pb–Zn–Cu–Au veins in Idaho, USA [52]; the Keketale Pb–Zn–(Ag) deposit and the Ashele Cu-Zn deposit in Altay in the western CAOB (Central Asian Orogenic Belt) [9,53]; Talate Pb–Zn deposit in Altay, China [54]; some base metal deposits in the Iberian Pyrite Belt, such as Neves Corvo VMS Cu deposit [55] and Tharsis VMS Cu–Zn–Pb deposit [56]; and the Falun pyritic Zn–Pb–Cu–(Au–Ag) sulfide

deposit in Bergslagen, Sweden [57]. The XMOB (Xing'an Mongolian Orogenic Belt), the Bainaimiao Cu–Au–Mo deposit located ~600 km northeast of the Jiashengpan, provides another case of shear zone-controlled base metal mineralization in a Devonian collisional setting. Ore-forming elements of this deposit are believed to have initially been enriched in a porphyry body intruded at ~465 Ma, and subsequently remobilized during Devonian (360 Ma) regional metamorphism, forming shear zone-controlled high-grade Cu orebodies via the activity of low-salinity carbon-rich metamorphic fluid [58,59].

In conclusion, the geochronological study of the Jiashengpan deposit provides evidence of a base metal mineralization deposit formed during Devonian orogeny in Inner Mongolia. Although it is difficult to generate base metal deposits via metamorphic devolatilization, orogenic belts provide a unique tectonic setting that facilitates remobilization and further enrichment of pre-enriched sub-economic lithological units. The case study of the Jiashengpan deposit illustrates the significance of orogenic activities in the formation of base metal resources with affinities of orogenic-type deposits.

7. Conclusions

(1) $^{39}Ar/^{40}Ar$ dating results show that mineralization of the Jiashengpan took place in the Devonian, ca. 380 Ma, which is an environment of collisional orogeny, as a response to the collision between NCC and SMM.

(2) Permian magmatic rocks (ca. 278 Ma) constrain the upper limit of the age of ore-formation at the Jiashengpan, and had no significant contribution to the mineralization process.

Author Contributions: Filed work and experiment were performed by R.-C.Z. and C.Y.; data analysis and original draft were accomplished by C.Y.; R.-C.Z., Y.-L.X., W.-B.L. reviewed and edited the draft.

Funding: This work is financially supported by State Key Research Plan (No. 2017YFC0601302), National Natural Science of Foundation of China (Nos., 41872078, 41502069, 41672067, and 41472072), Young Elite Scientists Sponsorship Program by CAST (YESS), and Fundamental Research Funds for the Central Universities (No. FRF-TP-18-017A3).

Acknowledgments: We would like to thank the State Key Laboratory of Lithospheric Evolution, Institute of Geology and Geophysics, CAS and the State Key Laboratory of Geological Processes and Mineral Resources, China University of Geosciences, Wuhan, China for helping with the $^{39}Ar/^{40}Ar$ dating and LA-ICP-MS zircon dating, respectively. We thank Jiashengpan Mining Ltd., Inner Mongolia, China for helping during filed work.

Conflicts of Interest: The authors declare no conflict of interest.

References

1. Lang, D.Y.; Zhang, X.J. Geological setting and genesis of the Jiashengpan Pb–Zn–S ore belt, Inner Mongolia. *Miner. Depos.* **1987**, *6*, 39–54, (in Chinese with English abstract).
2. Peng, R.M.; Zhai, Y.S.; Wang, Z.G. Ore-controlling synchronous faults of Mesoproterozoic Dongshengmiao and Jiashengpan SEDEX-type ore deposits, Inner Mongolia. *Earth Sci.* **2000**, *25*, 404–410, (in Chinese with English abstract).
3. Peng, R.M.; Zhai, Y.S. The characteristics of hydrothermal exhalative mineralization of the Langshan—Zhaertai belt, Inner Monogolia, China. *Geosci. Front.* **2004**, *11*, 257–268, (in Chinese with English abstract).
4. Fu, C. The Geological Features and Genesis of the Jiashengpan Lead–Zinc Deposit in Inner Mongolia, China. Master's Thesis, China University of Geosciences, Beijing, China, 2010.
5. Niu, S.Y.; Hu, X.; Xu, C.S. Geological features of ductile shear zone of chaertai group in Inner Mongolia. *J. Hebei Geo Univ.* **1990**, *2*, 147–156, (in Chinese with English abstract).
6. Zhong, R.C. The Potential of Forming Cu–Pb–Zn Deposits during Regional Metamorphism: Thermodynamic Modelling and a Case Study on the Langshan-Zhaertai Metallogenic Belt. Ph.D. Thesis, Peking University, Beijing, China, 2014.
7. Chen, Y.J. Orogenic-type deposit and their metallogenic model and exploration potential. *Chin. Geol.* **2006**, *33*, 1181–1196, (in Chinese with English abstract).
8. Pirajno, F. *Hydrothermal Processes and Mineral Systems*, 1st ed.; Springer: Berlin, Germany, 2009; pp. 1–1250.

9. Zheng, Y.; Zhang, L.; Chen, Y.J.; Hollings, P.; Chen, H.Y. Metamorphosed Pb–Zn–(Ag) ores of the Keketale VMS deposit, NW China: Evidence from ore textures, fluid inclusions, geochronology and pyrite compositions. *Ore Geol. Rev.* **2013**, *54*, 167–180. [CrossRef]
10. Phillips, G.N.; Powell, R. Formation of gold deposits: A metamorphic devolatilization model. *J. Metamorph. Geol.* **2010**, *28*, 689–718. [CrossRef]
11. Zhong, R.C.; Brugger, J.; Chen, Y.J.; Li, W.B. Contrasting regimes of Cu, Zn and Pb transport in ore-forming hydrothermal fluids. *Chem. Geol.* **2015**, *395*, 154–164. [CrossRef]
12. Peng, R.M.; Zhai, Y.S.; Han, X.F.; Wang, Z.G.; Wang, J.P.; Liu, J.J. Sinsedimentry volcanic activities in the cracking process of the Mesoproterozoic aulacogen of passive continental margin in Langshan-Zhaertai area, Inner Mongolia, and its indicating significance. *Acta Petrol. Sin.* **2007**, *23*, 1007–1017, (in Chinese with English abstract).
13. Peng, R.M.; Zhai, Y.S.; Wang, J.P.; Chen, X.F.; Liu, Q.; L, J.Y.; Shi, Y.X.; Wang, G.; Li, S.B.; Wang, L.G.; et al. Discovery of Neoproterozoic acid volcanic rock in the south-western section of Langshan, Inner Mongolia. *Chin. Sci. Bull.* **2010**, *55*, 2611–2620, (in Chinese with English abstract).
14. Gong, W.B.; Hu, J.M.; Li, Z.H.; Dong, X.P.; Liu, S.C. Detrital zircon U–Pb dating of Zhaertai Group in the North Margin Rift Zone of North China Craton and its implications. *Acta Petrol. Sin.* **2016**, *32*, 2151–2165, (in Chinese with English abstract).
15. Li, Q.L.; Chen, F.K.; Guo, J.H.; Li, X.H.; Yang, Y.H.; Siebel, W. Zircon ages and Nd–Hf isotopic composition of the Zhaertai Group (Inner Mongolia): Evidence for early Proterozoic evolution of the northern North China Craton. *J. Asian Earth Sci.* **2007**, *30*, 573–590. [CrossRef]
16. Hu, J.M.; Gong, W.B.; Wu, S.J.; Liu, Y.; Liu, S.C. LA-ICP-MS zircon U–Pb dating of the Langshan Group in the northeast margin of the Alxa block, with tectonic implications. *Precambrian Res.* **2014**, *255*, 756–770. [CrossRef]
17. Pi, Q.H.; Liu, C.Z.; Chen, Y.L.; Li, Y.Q.; Li, D.P. Formation epoch and genesis of intrusive rocks in Huogeqi orefield of Inner Mongolia and their relationship with copper mineralisation. *Miner. Depos.* **2010**, *29*, 437–451, (in Chinese with English abstract).
18. Liu, Y. Geochemical and Chronological Characteristics of the Granitic Gneisses and Intrusive Rocks from Dongshengmiao Ore District, Inner Mongolia and their Tectonic Implications. Master's Thesis, Lanzhou University, Lanzhou, China, 2012.
19. Wu, Y.F.; Zeng, J.N.; Cao, J.J.; Wu, Z.Q.; Chen, J.H.; Zhou, S.D.; Lu, S.F.; Li, X.F. Zircon U-Pb ages an Hf isotopes of Hercynia intrusion in Dongshengmiao, Inner Mongolia. *Geol. Sci. Technol. Inf.* **2013**, *32*, 22–30, (in Chinese with English abstract).
20. Hu, C.S.; Li, W.B.; Xu, C.; Zhong, R.C.; Zhu, F.; Qiao, X.Y. Geochemistry and petrogenesis of Permian granitoids in the northwestern margin of the North China Craton: Insights from the Dongshengmiao pluton, Inner Mongolia. *Int. Geol. Rev.* **2015**, *57*, 1843–1860. [CrossRef]
21. Qiao, X.Y.; Li, W.B.; Zhong, R.C.; Hu, C.S.; Zhu, F.; Li, Z.H. Elemental and Sr-Nd isotopic geochemistry of the Uradzhongqi magmatic complex in western Inner Mongolia, China: A record of early Permian post-collisional magmatism. *J. Asian Earth Sci.* **2017**, *144*, 171–183. [CrossRef]
22. Zhao, P.; Xu, B.; Zhang, C.H. A rift system in southeastern Central Asian Orogenic Belt: Constraint from sedimentological, geochronological and geochemical investigations of the Late Carboniferous-Early Permian strata in northern Inner Mongolia (China). *Gondwana Res.* **2017**, *47*, 342–357. [CrossRef]
23. Xiao, W.J.; Windley, B.F.; Hao, J.; Zhai, M.G. Accretion leading to collision and the Permian Solonker suture, Inner Mongolia, China: Termination of the central Asian orogenic belt. *Tectonics* **2003**, *22*. [CrossRef]
24. Xiao, W.J.; Windley, B.F.; Huang, B.C.; Han, C.M.; Yuan, C.; Chen, H.L.; Sun, M.; Sun, S.; Li, J.L. End-Permian to mid-Triassic termination of the accretionary processes of the southern Altaids: Implications for the geodynamic evolution, Phanerozoic continental growth, and metallogeny of Central Asia. *Int. J. Earth Sci.* **2009**, *98*, 1219–1220. [CrossRef]
25. Zhang, S.H.; Zhao, Y.; Song, B.; Hu, J.M.; Liu, S.W.; Yang, Y.H.; Chen, F.K.; Liu, X.M.; Liu, J. Contrasting Late Carboniferous and Late Permian—Middle Triassic intrusive suites from the northern margin of the North China craton: Geochronology, petrogenesis, and tectonic implications. *Geol. Soc. Am. Bull.* **2009**, *121*, 181–200. [CrossRef]

26. Xu, B.; Charvet, J.; Chen, Y.; Zhao, P.; Shi, G.Z. Middle Paleozoic convergent orogenic belts in western Inner Mongolia (China): Framework, kinematics, geochronology and implications for tectonic evolution of the Central Asian Orogenic Belt. *Gondwana Res.* **2013**, *23*, 1342–1364. [CrossRef]
27. Xu, B.; Zhao, P.; Bao, Q.Z.; Zhou, Y.H.; Wang, Y.Y.; Luo, Z.W. Preliminary study on the pre-Mesozoic tectonic unit division of the Xing-Meng Orogenic Belt (XMOB). *Acta Petrol. Sin.* **2014**, *30*, 1841–1857, (in Chinese with English abstract).
28. Shao, J.A.; Tang, K.D.; He, G.Q. Early Permian tectono-palaeogeographic reconstruction of Inner Mongolia, China. *Acta Petrol. Sin.* **2014**, *30*, 1858–1866, (in Chinese with English abstract).
29. Shao, J.A.; He, G.Q.; Tang, K.D. The evolution of Permian continental crust in northern part of North China. *Acta Petrol. Sin.* **2015**, *31*, 47–55, (in Chinese with English abstract).
30. Jian, P.; Liu, D.Y.; Kroner, A.; Windley, B.F.; Shi, Y.R.; Zhang, W.; Zhang, F.Q.; Miao, L.C.; Zhang, L.Q.; Tomurhuu, D. Evolution of a Permian intraoceanic arc-trench system in the Solonker suture zone, Central Asian Orogenic Belt, China and Mongolia. *Lithos* **2010**, *118*, 169–190. [CrossRef]
31. Chen, Y.P.; Wei, C.J.; Zhang, J.R.; Chu, H. Metamorphism and zircon U–Pb dating of garnet amphibolite in the Baoyintu Group, Inner Mongolia. *Sci. Bull.* **2015**, *60*, 1698–1707. [CrossRef]
32. Chu, H.; Zhang, J.R.; Wei, C.J.; Wang, H.C.; Ren, Y.W. A new interpretation of the tectonic setting and age of meta-basic volcanics in the Ondor Sum Group, Inner Mongolia. *Chin. Sci. Bull.* **2013**, *58*, 3580–3587, (in Chinese with English abstract). [CrossRef]
33. Zhang, J.R.; Chu, H.; Wei, C.J.; Wang, K. Geochemical characteristics and tectonic significance of Late Paleozoic-Early Mesozoic meta-basic rocks in the melange zones, Central Inner Mongolia. *Acta Petrol. Sin.* **2014**, *30*, 1935–1947, (in Chinese with English abstract).
34. Song, S.G.; Wang, M.M.; Xu, X.; Wang, C.; Niu, Y.L.; Allen, M.B.; Su, L. Ophiolites in the Xing'an-Inner Mongolia accretionary belt of the CAOB: Implications for two cycles of seafloor spreading and accretionary orogenic events. *Tectonics* **2015**, *34*, 2221–2248. [CrossRef]
35. Zhang, J.R.; Wei, C.J.; Chu, H. New model for the tectonic evolution of Xing'an-Inner Mongolia Orogenic Belt: Evidence from four different phases of metamorphism in Central Inner Mongolia. *Acta Petrol. Sin.* **2018**, *34*, 2857–2872, (in Chinese with English abstract).
36. Baksi, A.K.; Archibald, D.A.; Farrar, E. Use of a double-spike to determine the half-life of 39Ar and the operating characteristics of a mass spectrometer used in geochronological studies. *Can. J. Phys.* **1996**, *74*, 263–266. [CrossRef]
37. Koppers, A.A.P. ArArCALC-software for $^{40}Ar/^{39}Ar$ age calculations. *Comput. Geosci.* **2002**, *28*, 605–619. [CrossRef]
38. Dalrymple, G.B.; Lanphere, M.A. $^{40}Ar/^{39}Ar$ technique of K–Ar dating: A comparison with the conventional technique. *Earth Planet. Sci. Lett.* **1971**, *12*, 300–308. [CrossRef]
39. Fleck, R.J.; Sutter, J.F.; Elliott, D.H. Interpretation of discordant $^{40}Ar/^{39}Ar$ age-spectra of Mesozoic tholeiites from Antarctica. *Geochim. Cosmochim. Acta* **1977**, *41*, 15–32. [CrossRef]
40. Yuan, H.; Gao, S.; Liu, X.; Li, H.; Günther, D.; Wu, F. Accurate U–Pb age and trace element determinations of zircon by laser ablation-inductively coupled plasma-mass spectrometry. *Geostand. Geoanal Res.* **2004**, *28*, 353–370. [CrossRef]
41. Andersen, T. Correction of common lead in U–Pb analyses that do not report ^{204}Pb. *Chem. Geol.* **2002**, *192*, 59–79. [CrossRef]
42. Liu, Y.S.; Gao, S.; Hu, Z.C.; Gao, C.G.; Zong, K.Q.; Wang, D.B. Continental and oceanic crust recycling-induced melt-peridotite interactions in the trans-north China orogen: U–Pb dating, Hf Isotopes and trace elements in zircons from mantle xenoliths. *J. Petrol.* **2010**, *51*, 537–571. [CrossRef]
43. Ludwig, K. User's manual for IsoPlot 3.0. In *A Geochronological Toolkit for Microsoft Excel*; Berkeley Geochronology Center: Berkeley, CA, USA, 2003; p. 71.
44. McDougall, I.; Mac Dougall, I.; Harrison, T.M. *Geochronology and Thermochronology by the $^{40}Ar/^{39}Ar$ Method*, 2nd ed.; Oxford University: Oxford, UK, 1999; pp. 1–269.
45. Belousova, E.A.; Griffin, W.L.; O'Reilly, S.Y.; Fisher, N.I. Igneous zircon: Trace element composition as an indicator of source rock type. *Contrib. Mineral. Petrol.* **2002**, *143*, 602–622. [CrossRef]
46. Goldfarb, R.; Baker, T.; Dube, B.; Groves, D.I.; Hart, C.J.; Gosselin, P. Distribution, character and genesis of gold deposits in metamorphic terranes. *Econ. Geol.* **2005**, *2005*, 407–450.

47. Goldfarb, R.J.; Groves, D.I.; Gardoll, S. Orogenic gold and geologic time: A global synthesis. *Ore. Geol. Rev.* **2001**, *18*, 1–75. [CrossRef]
48. Hart, C.J.R.; Goldfarb, R.J.; Qiu, Y.M.; Snee, L.; Miller, L.D.; Miller, M.L. Gold deposits of the northern margin of the North China Craton: Multiple late Paleozoic-Mesozoic mineralizing events. *Miner. Depos.* **2002**, *37*, 326–351. [CrossRef]
49. Miao, L.C.; Qiu, Y.M.; McNaughton, N.; Fan, W.M.; Groves, D.I.; Zhai, M.G. SHRIMP U-Pb zircon ages of granitoids in the Wulashan gold deposit, inner Mongolia, China: Timing of mineralization and tectonic implications. *Int. Geol. Rev.* **2003**, *45*, 548–562. [CrossRef]
50. Pitcairn, I.K.; Teagle, D.A.H.; Craw, D.; Olivo, G.R.; Kerrich, R.; Brewer, T.S. Sources of metals and fluids in orogenic gold deposits: Insights from the Otago and Alpine schists, New Zealand. *Econ. Geol.* **2006**, *101*, 1525–1546. [CrossRef]
51. Marshall, B.; Vokes, F.M.; Larocque, A.C.L. Regional metamorphic remobilisation: Upgrading and formation of ore deposits. *Rev. Econ. Geol.* **2000**, *11*, 19–38.
52. Leach, D.L.; Landis, G.P.; Hofstra, A.H. Metamorphic origin of the Coeur d'Alene base-and precious-metal veins in the Belt basin, Idaho and Montana. *Geology* **1988**, *16*, 122–125. [CrossRef]
53. Zheng, Y.; Wang, Y.J.; Chen, H.Y.; Lin, Z.W.; Hou, W.S.; Li, D.F. Micro-textural and fluid inclusion data constraints on metallic remobilization of the Ashele VMS Cu–Zn deposit, Altay, NW China. *J. Geochem. Explor.* **2016**, *171*, 113–123. [CrossRef]
54. Zhang, H.; Xu, J.H.; Guo, X.J.; Xiao, X.; Un, L.H.; Yang, R.; Cheng, X.H. Metamorphic overprints on the Talate Pb–Zn deposit in Altay: Evidences from geology and fluid inclusions. *Acta Petrol. Sin.* **2015**, *31*, 1063–1078.
55. Moura, A. Metamorphosed and metamorphogenic ores of the Neves Corvo volcanogenic massive sulfide deposit, Iberian Pyrite Belt, Portugal. *Int. Geol. Rev.* **2008**, *50*, 89–96. [CrossRef]
56. Marignac, C.; Diagana, B.; Cathelineau, M.; Boiron, M.C.; Banks, D.; Fourcade, S.; Vallance, J. Remobilisation of base metals and gold by Variscan metamorphic fluids in the south Iberian pyrite belt: Evidence from the Tharsis VMS deposit. *Chem. Geol.* **2003**, *194*, 143–165. [CrossRef]
57. Kampmann, T.C.; Jansson, N.J.; Stephens, M.B.; Olin, P.H.; Gilbert, S.; Wanhainen, C. Syn-tectonic sulphide remobilization and trace element redistribution at the Falun pyritic Zn–Pb–Cu–(Au–Ag) sulphide deposit, Bergslagen, Sweden. *Ore Geol. Rev.* **2018**, *96*, 48–71. [CrossRef]
58. Li, W.B.; Chen, Y.J.; Lai, Y.; Ji, J.Q. Metallogenic time and tectonic setting of the Bainaimiao Cu–Au deposit, Inner Mongolia. *Acta Petrol. Sin.* **2008**, *24*, 890–898, (in Chinese with English abstract).
59. Li, W.B.; Hu, C.S.; Zhong, R.C.; Zhu, F. U–Pb, $^{39}Ar/^{40}Ar$ geochronology of the metamorphosed volcanic rocks of the Bainaimiao Group in central Inner Mongolia and its implications for ore genesis and geodynamic setting. *J. Asian Earth Sci.* **2015**, *97*, 251–259. [CrossRef]